Transcranial alternating current stimulation entrains single-neuron activity in the primate brain

Matthew R. Krause[a,1], Pedro G. Vieira[a,1], Bennett A. Csorba[a], Praveen K. Pilly[b], and Christopher C. Pack[a,2]

[a]Montreal Neurological Institute, McGill University, Montreal, QC H3A 2B4, Canada; and [b]Information and Systems Sciences Laboratory, HRL Laboratories, Malibu, CA 90265

Edited by Robert Desimone, Massachusetts Institute of Technology, Cambridge, MA, and approved February 6, 2019 (received for review September 14, 2018)

Spike timing is thought to play a critical role in neural computation and communication. Methods for adjusting spike timing are therefore of great interest to researchers and clinicians alike. Transcranial electrical stimulation (tES) is a noninvasive technique that uses weak electric fields to manipulate brain activity. Early results have suggested that this technique can improve subjects' behavioral performance on a wide range of tasks and ameliorate some clinical conditions. Nevertheless, considerable skepticism remains about its efficacy, especially because the electric fields reaching the brain during tES are small, whereas the likelihood of indirect effects is large. Our understanding of its effects in humans is largely based on extrapolations from simple model systems and indirect measures of neural activity. As a result, fundamental questions remain about whether and how tES can influence neuronal activity in the human brain. Here, we demonstrate that tES, as typically applied to humans, affects the firing patterns of individual neurons in alert nonhuman primates, which are the best available animal model for the human brain. Specifically, tES consistently influences the timing, but not the rate, of spiking activity within the targeted brain region. Such effects are frequency- and location-specific and can reach deep brain structures; control experiments show that they cannot be explained by sensory stimulation or other indirect influences. These data thus provide a strong mechanistic rationale for the use of tES in humans and will help guide the development of future tES applications.

tES | tACS | transcranial alternating current stimulation | spike timing | phase-locking

When a neuron fires a volley of action potentials, information may be encoded in the precise timing of spikes as well as the overall firing rate. Moreover, spike timing may convey information that is not accessible from a rate code. In the hippocampus, the timing of spikes provides precise information about an individual's position (1); similar mechanisms may control perceptual organization in visual cortex as well (2). At a larger scale, the fine temporal structure of neural signals is thought to provide a mechanism for flexibly routing information according to behavioral demands (3). As changes in the temporal structure of neural activity appear to underlie momentary lapses in performance (4) and serious pathological conditions (5), there has been considerable interest in understanding the factors that influence spike timing.

Recently, transcranial electrical stimulation (tES) has become a popular tool for clinicians and researchers seeking to noninvasively alter brain states. Electrodes are placed on a subject's scalp, and a weak electric current is passed among them, generating an electric field that, in theory, passes through the skull and interacts with the electrical activity of the neurons beneath. Early results suggested that this simple technique could alter healthy subjects' perceptual, cognitive, and emotional states and relieve a wide variety of disease symptoms in patients (6–8).

However, these results have been met with some skepticism. Subsequent meta-analyses have suggested that the behavioral effects of tES can be weak or highly variable (9–12). Furthermore, a clear neural mechanism by which tES can influence human behavior has yet to be identified. Previous studies have used in vitro (13, 14) or small animal preparations (15) that are difficult to translate to humans, as the experiments typically use highly invasive stimulation techniques and apply very strong electric fields. Extrapolation from these studies is further complicated by the fact that humans have thicker, bonier skulls and larger, gyrated brains, which attenuate and distort the fields produced during tES (16, 17). Taking these factors into consideration, Vöröslakos et al. (18) recently estimated that 75% of the current applied during tES never reaches the human brain as a result of shunting through the scalp; they concluded that the electric fields inside the skull are too feeble to affect neural activity. Based on these and similar studies, it has been suggested that the behavioral effects of tES are likely the results of nonspecific mechanisms, such as the placebo effect (19) or activation of peripheral nerves (20).

Ultimately, any intervention that seeks to modify brain function must affect single neuron activity. Furthermore, the nature of many clinical or research applications requires the ability to target specific brain structures. Both of these criteria can be tested most effectively in nonhuman primates, which, like humans, have thick skulls and large, gyrencephalic brains. To date, only a few studies have applied tES to nonhuman primates with noninvasive approaches that resemble those used in human experiments. These studies reported changes in secondary markers of neural activity, such as local field potentials, functional connectivity, and stimulus selectivity (21–23), rather than changes in the activity of individual neurons. Similarly, intracranial recordings from humans have generally lacked

Significance

Neurostimulation is a common therapy for a variety of neurological disorders, but the most effective stimulation approaches are often highly invasive, requiring electrodes to be implanted deep within brain structures like the hippocampus and basal ganglia. Here, we show that transcranial electrical stimulation (tES), a neuromodulatory technique that uses electrodes placed outside the scalp, can also affect patterns of neural activity in these areas. We find that tES can reliably control the timing, but not the rate, of spikes in individual neurons. Because changes in spike timing are thought to play a key role in many brain functions, the data shown here suggest that tES may be a valuable tool for clinical and fundamental studies of the human brain.

Author contributions: M.R.K., P.G.V., P.K.P., and C.C.P. designed research; M.R.K., P.G.V., and B.A.C. performed research; M.R.K. and P.G.V. analyzed data; and M.R.K., P.G.V., P.K.P., and C.C.P. wrote the paper.

Conflict of interest statement: P.K.P. has filed invention disclosures and has pending patent applications on other techniques and applications of noninvasive brain stimulation. The remaining authors declare no competing interests.

This article is a PNAS Direct Submission.

[1]M.R.K. and P.G.V. contributed equally to this work.

[2]To whom correspondence should be addressed. Email: christopher.pack@mcgill.ca.

This article contains supporting information online at www.pnas.org/lookup/suppl/doi:10.1073/pnas.1815958116/-/DCSupplemental.

Published online March 4, 2019.

the ability to resolve single-neuron activity (24). Thus, it remains unclear whether and how tES affects neuronal activity in the primate brain.

To address these issues, we recorded the activity of single neurons from the brains of alert nonhuman primates while applying tES methods identical to those used in humans. Our results confirm that the resulting electric field actually reaching the brain is weak, and that it does not change the firing rates of single neurons. However, we find that tES reliably alters single-neuron spike timing, even in deep brain structures distant from the sites of stimulation on the scalp. These effects are not consistent with activation via nonspecific or indirect pathways, but suggest a direct effect on neurons near the targeted area. These data show that tES can reliably modulate neural activity and provide important constraints for the future design of research and therapeutic interventions.

Results

Our experiments focus on transcranial alternating current stimulation (tACS), a form of tES that uses alternating current to generate oscillating electric fields. Previous work has suggested that tACS might exert two broad classes of influences on neural activity: changes in firing rate (25, 26) and changes in spike timing (27, 28). To investigate these possible effects, we applied tACS through the scalps of two macaque monkeys while recording single-unit activity from the hippocampus, a popular target in rodent (15, 29) and slice studies (30), as well as a frequent target for invasive stimulation in humans (31–35). We also recorded from neurons in the nearby basal ganglia (BG), which is similarly of interest as a therapeutic target for brain stimulation (36, 37).

tACS Produces Weak Electric Fields in the Primate Brain. We first sought to identify scalp locations for the tACS electrodes that delivered field strengths similar to those observed in human experiments. To this end, we built individualized models of each animal's head from high-resolution MRIs and intraoperative records of implant locations [see Datta et al. (38) and *SI Appendix*, *SI Materials and Methods*], which were then solved to find electrode montages that generated appropriate electric field strengths around the recording sites. We considered montages containing as many as eight electrode sites, with a total current budget of ±2 mA (4 mA peak to peak) across the entire montage, as is typical in human tES experiments. The resulting field strengths were estimated from the model to be 0.29 V/m in monkey F and 0.26 V/m in monkey N.

Consistent with these predictions, we measured peak field strengths of 0.28 V/m in monkey F and 0.35 V/m in monkey N. The mean ± SE of the field strengths in the two monkeys were 0.23 ± 0.01 and 0.19 ± 0.02 V/m, respectively. These are comparable to, and, in fact, slightly lower than, values reported in human studies, which can reach as high as 0.8 V/m (16, 17), albeit at sites closer to the brain's surface.

tACS Alters Spike Timing in Deep Brain Structures. Next, we used these stimulation montages to investigate how tACS affects single-unit activity. The animals performed a simple visual fixation task while we recorded single-unit activity (*Methods*) and applied tACS. Two kinds of stimulation were applied in randomly interleaved 5-min blocks. During active tACS blocks, the stimulation consisted of a ±2-mA sine wave oscillating at 5, 10, 20, or 40 Hz. During sham blocks, we applied only the onset and offset of the active tACS waveform (*Methods*). This latter approach mimics the sensations evoked by tACS so well that human subjects are generally unable to distinguish between them (39–41), and thus serves as a useful control for nonspecific sensory effects of stimulation. Blocks were separated by a 5-min interstimulus interval, and 6–10 blocks were collected per session.

We recorded from a total of 197 cells: 136 from the BG and 61 from HC. The BG neurons came from monkey F (89 cells; 65%) and monkey N (47 cells; 35%), whereas all 61 hippocampal neurons were recorded from monkey N. These recording locations were confirmed by aligning postoperative CT scans, with the electrodes inserted, to the preoperative MRI scans (*SI Appendix*, Fig. S1).

Data from an example BG neuron are shown in Fig. 1*A*. The raster plot on the left shows the neuron's spiking activity during 10 1-s segments taken from a block of 20-Hz active tACS (Fig. 1*A*, orange) and sham stimulation (Fig. 1*A*, blue). There was no obvious difference in this neuron's firing rate between stimulation conditions in these example intervals, nor, as shown in column *2*, across the entire experimental session ($P = 0.37$, mixed-effects model). At the same time, it is clear that the timing of the spikes became more regular during tACS, with the neuron preferentially firing at the beginning of each tACS cycle (Fig. 1*A*, black trace at top), when the phase was around zero degrees (Fig. 1*A*, gray lines).

To quantify this entrainment, we computed the phase-locking value (PLV), which provides a measure of the reliability of spike times relative to an oscillation, in this case the waveform of the tACS stimulation. A PLV of zero means that spike times are uniformly distributed across the tACS cycle, whereas a value of one means that spikes appear exclusively at a single phase. For the neuron shown in Fig. 1*A*, the PLVs were 0.003 during sham stimulation and 0.73 during tACS; a randomization test reveals that this increase was statistically significant ($P = 0.004$).

Fig. 1 *B*–*D* shows three other example neurons, also recorded from the BG. As in Fig. 1*A*, none of the neurons showed a significant change in firing rate between the sham and active stimulation conditions ($P = 0.23$, $P = 0.75$, and $P = 0.72$, respectively, via a mixed-effects model). However, the cells in Fig. 1 *B* and *C* exhibited modest entrainment to the tACS, whereas the neuron in Fig. 1*D* appears to be unaffected. Note that the neurons in Fig. 1 *C* and *D* were recorded simultaneously on neighboring channels 150 μm apart, suggesting that the effects of tACS can be heterogeneous, even very locally within the stimulated area.

To ensure that our recordings were stable throughout the active and sham stimulation blocks, we plotted spike waveforms separately for each condition. These are shown for the example neurons in the rightmost column of Fig. 1. The thick orange lines show the units' average waveform during active tACS application, superimposed on error bars derived from the sham data (Fig. 1, *Right*, light blue band). The average sham waveform is also shown (Fig. 1, *Right*, thick blue line) superimposed against the error bars from the tACS condition (Fig. 1, *Right*, orange band). Spike waveforms appear very similar across conditions. To quantify this similarity for the population, we calculated the median correlation between neurons' average waveforms during tACS and sham blocks. The overall correlation was very high ($r_s = 0.993$), indicating that spike waveforms were stable across conditions. As shown in *SI Appendix*, Fig. S2, the waveforms were also extremely stable across tACS phases, indicating that the entrainment is not a result of a loss of signal during part of the stimulus cycle.

Fig. 2 summarizes firing rate and entrainment effects across our data set for all stimulation frequencies. Firing rates were very similar in the sham and active stimulation conditions (Fig. 2*A*). At the single-cell level, only 14 of 197 cells (7%) showed individually significant changes in firing rate (mixed-effects models, $P < 0.05$). These were evenly distributed across the frequencies tested ($n = 4$, $n = 4$, $n = 2$, and $n = 4$ cells, respectively), and, even though decreases in firing rate were slightly more common ($n = 9$ cells) than increases ($n = 5$ cells), there was no statistical evidence of a preferred sign for these changes [$\chi(1)^2 = 0.58$; $P = 0.45$]. As cells were individually assessed at the $P = 0.05$ level, we would expect to see between 4 and 17 modulated cells by chance alone, so we interpret these firing rate changes as type II errors rather than an effect of tACS. Across the population of neurons recorded in each condition (*SI Appendix*, Fig. S3), the median changes in firing rate were not significantly different at any frequency ($P > 0.05$, Wilcoxon signed-rank

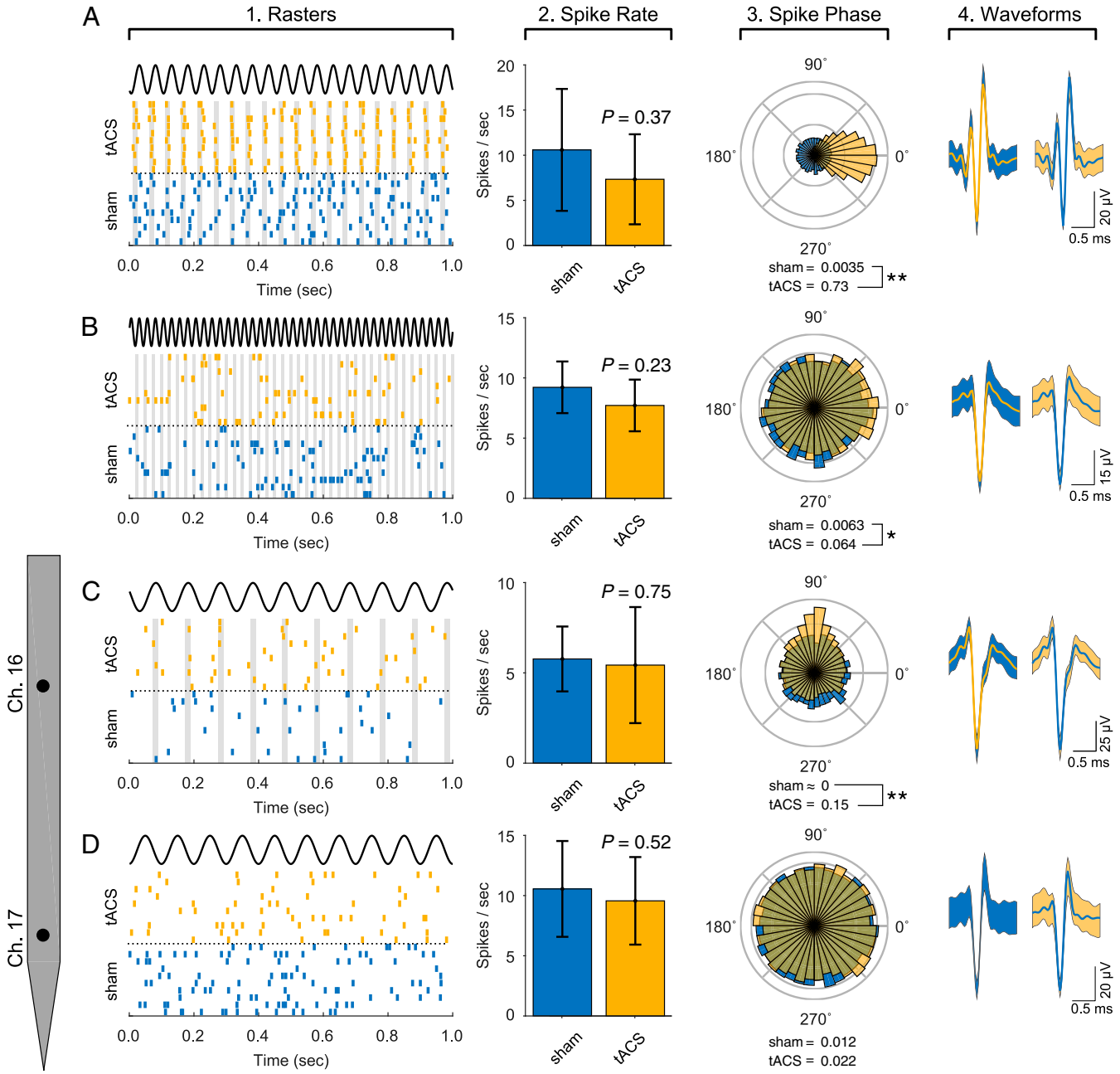

Fig. 1. Example neurons demonstrating the range of responses to tACS. Each row contains data from a single neuron during 20-Hz (*A*), 40-Hz (*B*), and 10-Hz tACS (*C* and *D*), along with the corresponding sham conditions. The schematic electrode indicates that the neurons in *C* and *D* were recorded simultaneously on adjacent channels. Neurons in *A* and *B* were recorded during separate sessions. Column *1* contains raster plots from 10 1-s segments of the data, showing the tACS waveform (black), spikes occurring during tACS (orange), and spikes occurring during sham trials (blue). Vertical gray lines denote each neuron's preferred phase during tACS; these are omitted in *D* because the neuron had no preferred phase. Column *2* shows firing rates for each condition estimated by binning the cell's responses into 30-s windows. Average firing rates across conditions were then compared via a mixed-effects model test, the results of which are shown in the upper right. Column *3*: spike density plots show the relative probability of a spike at each phase of the tACS waveform (orange) or the corresponding LFP frequency band during sham trials (blue). To quantify the strength of the phase locking, PLVs are shown beneath each plot, as is the result of a randomization test comparing the PPC values between conditions. Asterisks indicate statistical significance (*$P < 0.05$ and **$P < 0.01$). Column *4*: left traces show the average waveform during tACS (thick orange line) superimposed over a band depicting the mean ± SD of the waveform during sham stimulation (blue band). Traces on the right show the average waveform during sham stimulation (thick blue line) superimposed over a band indicating the mean ± SD of the waveform during tACS (orange band). *SI Appendix*, Fig. S1 shows recording sites, and *SI Appendix*, Fig. S2 shows additional waveforms.

tests). Thus, there was no consistent evidence for an effect of tACS on firing rate for individual cells or for the population of cells.

In contrast, we found considerable evidence for the entrainment of single-unit activity by tACS (Fig. 2*B*). At the single-cell level, we used a randomization test to determine whether PLV values significantly changed between the stimulation and sham conditions (*Methods*). Overall, 44%, or 86 of 197 neurons, showed individually significant PLV changes at the $P = 0.05$ level. Of these, the vast majority of cells (77 of 86, or 90%) were more strongly entrained during tACS [$\chi(1)^2 = 30$; $P < 0.001$]. The distribution of modulated cells did not differ across the tested frequencies (Fisher's exact test, $P = 0.25$).

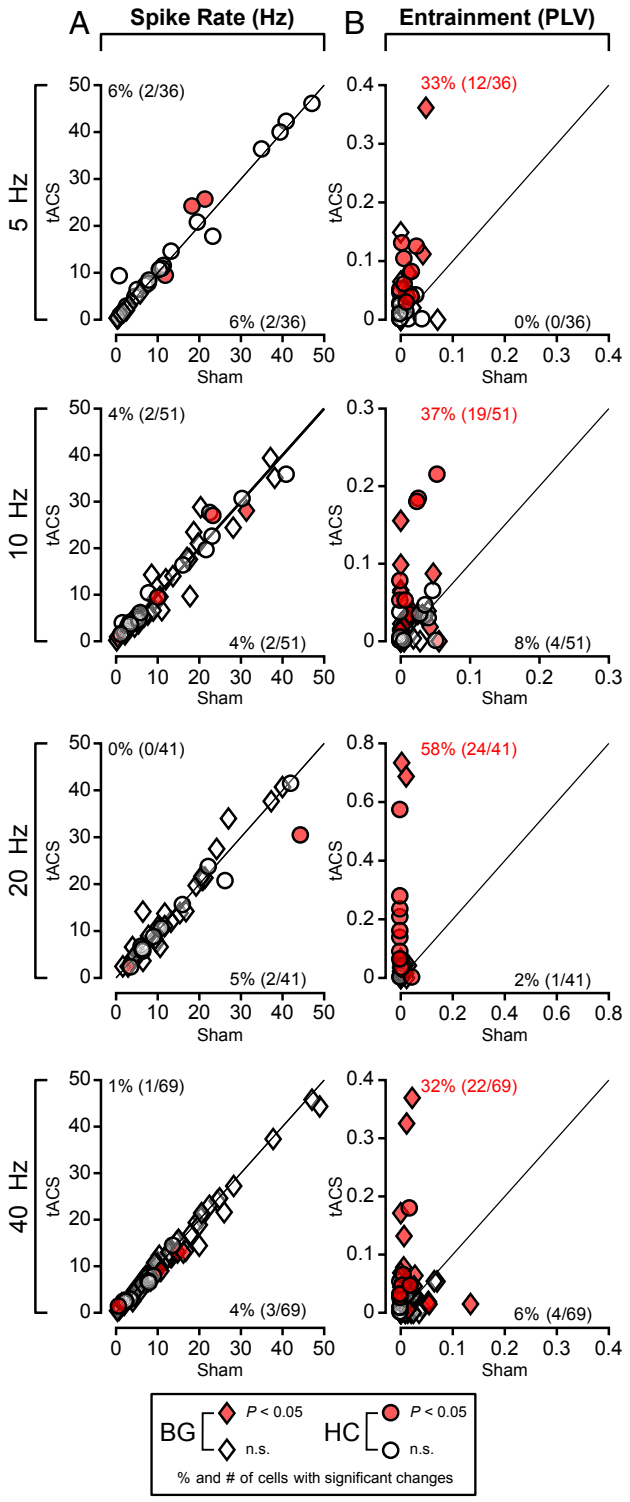

Fig. 2. Population distributions for firing rates and PLVs. (*A*) Distributions of average firing rate during 5-Hz, 10-Hz, 20-Hz, and 40-Hz tACS. Each point compares a single neuron's firing rate during sham stimulation (*x*-axis) and active tACS (*y*-axis). Rates were distributed along the equality line, indicating that firing rates did not change across conditions. The percentage of cells exhibiting significant changes for active tACS vs. sham is indicated on the top (increases) or bottom (decreases) corners of each graph, respectively. Red text indicates that proportions are larger than would be expected by chance (i.e., outside the 95% binomial CI). (*B*) PLVs presented in the same style as *A*. Unlike the firing rates, PLV values tend to be above the diagonal line, indicating a strengthening of entrainment during active tACS. *SI Appendix*, Fig. S3 shows population effect sizes.

To examine these effects at the population level, we computed the median change in PLV (i.e., tACS − sham) for each cell and each frequency of stimulation. Overall, changes in PLV were significantly larger than zero for all frequencies (5 Hz, $Z = 3.7$, $P < 0.0004$; 10 Hz, $Z = 3.2$, $P < 0.003$; 20 Hz, $Z = 4.6$, $P < 0.00004$; 40 Hz, $Z = 3.0$, $P = 0.0052$, right-tailed Wilcoxon signed-rank tests; *SI Appendix*, Fig. S3). However, there was a statistical effect of stimulation frequency on the change in PLV [Kruskal–Wallis test, $\chi^2(3) = 13.7$, $P = 0.033$], driven primarily by the relative weakness of 40-Hz tACS compared with the remaining frequencies, particularly 5 Hz ($P = 0.06$, post hoc, Dunn–Šidák corrected) and 20 Hz ($P = 0.0092$). The numerically largest effect of tACS was found for 20-Hz tACS in HC, in which the median PLV reached 0.11, but this effect was not significantly larger ($P = 0.12$, corrected Wilcoxon rank-sum test) than the same conditions in BG. Overall, the effects of tACS on firing rate and entrainment were similar between the two areas, as shown in Fig. 2 and detailed in *SI Appendix*, Table S1.

The tACS field is generated by a sinusoidal current and therefore reaches its maximum strength at 90°. If the external field were very strong, or the only input to the cell, neurons should be precisely phase-locked to this peak, as reported by Ozen et al. (15). By comparison, the relatively weak fields in our experiments did not completely override neurons' intrinsic phase preferences, as the preferred phases across the population remained scattered across the stimulus cycle ($\sigma^2_{\text{circular}} = 0.89$, $P = 0.38$). However, consistent with the expected biophysics, the phase preferences of the neurons that individually showed significant entrainment clustered around 90° ($P = 0.03$, Rayleigh's V test with $\Theta_0 = 90°$), where the field's polarizing influence was strongest. This clustering did not occur for the subset of neurons with significant entrainment during sham stimulation ($P = 0.90$, Rayleigh's V test with $\Theta_0 = 90°$). Although neurons with phase preferences near the peak (90 ± 45°) were entrained more strongly (ΔPLV = 0.052) than those with other phase preferences (ΔPLV = 0.034), this difference was not statistically significant ($P = 0.12$, $Z = 1.56$, Wilcoxon rank-sum tests).

At an even finer temporal scale, we observed an effect of tACS on the prevalence of bursting activity in single neurons. Bursts are neuronal responses in which two or more spikes are elicited in quick succession, and they are thought to reflect intrinsic membrane currents (42) that can, in principle, be modulated by tACS (43). To test for potential effects of tACS on bursting, we calculated a bursting index by dividing the average number of spikes in the 3–5-ms bins of the spike autocorrelogram by the average number of spikes in the 100–200-ms bins. Across the entire data set, bursting decreased from a median of 0.35 [interquartile range (IQR), 0.11–1.06] during sham stimulation to 0.30 (IQR, 0.12–0.89) during tACS; this effect was at the threshold of statistical significance ($P = 0.0529$, Wilcoxon signed-rank test). However, the low burst index values indicate that many cells do not burst in either condition, so we restricted our analysis to the 71 cells that exhibited bursting (i.e., burst index > 1). For these cells, the median burst index was 2.99 (IQR, 1.65–4.49) during sham stimulation but significantly decreased during tACS to 2.57 (IQR, 1.35–4.02; $P = 0.023$, Wilcoxon signed-rank test).

Cells may have differing susceptibility to external electric fields, as a consequence of a number of biophysical factors. One such factor is cellular morphology, which has been shown in slice recordings to be predictive of spiking responses to electrical fields (26). Although we cannot directly recover morphology from extracellular recordings, it is often linked to cell type (44). Accordingly, we divided our data set into putative interneurons and putative pyramidal cells according to their action potential width, using a threshold of 200 μs (44). However, we found no significant difference in phase-locking during tACS between the neuron clusters ($P = 0.77$, $Z = 0.29$).This may be because the HC and BG contain neurons at all orientations in close proximity (45); their

orientation relative to the electric field (13, 26) may mask any cell-type–specific effects. Furthermore, the GABAergic neurons in the deep brain are more morphologically similar to projection neurons than their cortical counterparts (46–48).

A second factor is overall excitability, which might be expected to determine a cell's sensitivity to electrical fields. However, there was also no relationship between neuronal excitability (as measured by firing rate) and changes in PLV in response to tACS ($r_s = 0.06$, $P = 0.32$). At the same time, we did find a modest association between a neuron's PLV during sham stimulation and the subsequent change in PLV during tACS ($r_s = 0.18$, $P = 0.0094$), which suggests that some cells have a propensity to become coupled to external oscillations (49).

The Effects of tACS Are Specific to the Targeted Location and Frequency. Merely changing spiking activity is necessary but not sufficient for tACS to be useful, as many proposed applications rely on the ability to target specific brain regions, often in specific frequency bands. We therefore examined the specificity of the observed spike timing effect in space and in frequency.

We first tested the frequency specificity of the tACS effects by extending our phase-locking analysis to all frequencies between 1 and 100 Hz (in ±1-Hz bins). Fig. 3*A* shows the median PLVs for 5-, 10-, 20-, and 40-Hz stimulation, with the blue lines corresponding to sham stimulation and the orange lines to tACS. In each case, entrainment effects, indicated by the horizontal line segment in each panel, were found only at frequencies near those of the stimulation frequency (e.g., 10 Hz for 10-Hz tACS; $P < 0.01$, Wilcoxon signed-rank tests); no significant changes were observed at any other frequency.

Next, we examined the spatial specificity of tACS effects. In these experiments, we applied the same stimulation montage as before while also recording from the left inferotemporal cortex (area TEO), a superficial visual area that is ∼20 mm away from the targeted areas. Fig. 3*B* shows that there was no consistent entrainment in TEO at any frequency during tACS. Data from individual TEO neurons are shown in *SI Appendix*, Fig. S4. Of the 21 TEO cells recorded, only three (14%) showed individually significant changes in entrainment as a result of tACS, which is significantly different ($\chi^2 = 6.2$, $P = 0.01$) from the distribution observed in HC and BG. Furthermore, two of those three cells showed significantly decreased entrainment during 10-Hz tACS, which is again different from the data from the targeted regions, where 90% of cells showed increased entrainment during tACS. Unlike in the targeted regions, stimulation did not affect the PLV of TEO neurons ($P = 0.877$, $Z = -0.15$, Wilcoxon signed-rank test), and the median change in TEO neurons' PLV was 0, significantly smaller than that recorded in the targeted regions ($P = 0.0042$, $Z = -2.86$). This demonstrates that neurons far from the targeted areas are not affected by tACS.

We further tested for spatial specificity by recording from the same brain regions (BG and HC) as before while changing the configuration of the stimulation montage. In these experiments, the electrode montage was mirrored across the midline, so that the strongest stimulation would no longer be expected to reach the brain regions near the recording electrodes. Fig. 4*A* compares the entrainment produced by the original optimized montages (Fig. 4*A*, *Left*; $n = 18$ neurons) and mirrored montages (Fig. 4*A*, *Right*; $n = 20$ neurons), along with the corresponding sham controls. As before, the optimal montage entrained neurons significantly more effectively ($P = 0.026$, Wilcoxon signed-rank test) than the sham control. However, entrainment was unchanged at all frequencies ($P > 0.05$) when tACS and sham stimulation were applied through the mirrored montage. Similar results were obtained with 20-Hz stimulation (optimal, $n = 12$; mirrored, $n = 8$): the optimal montage produced a significant increase in entrainment around 20 Hz ($P = 0.005$, Wilcoxon signed-rank test), but tACS and sham stimulation applied through the mirrored montages were again equally ineffective ($P > 0.05$) at all frequencies.

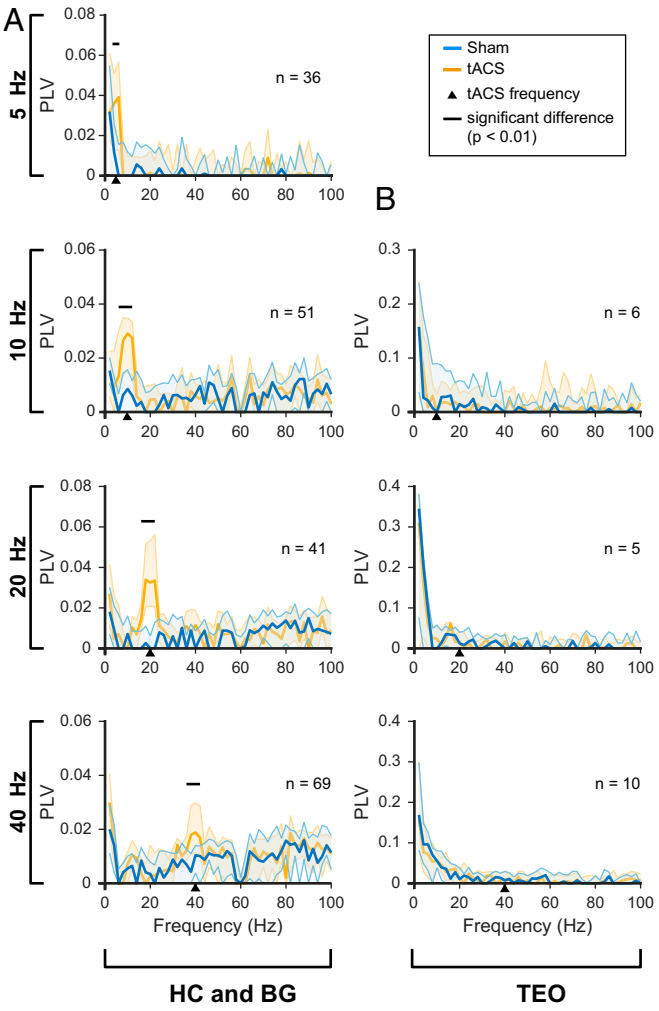

Fig. 3. (*A*) Neurons in the targeted area entrain only to the stimulation frequency. To test for possible cross-frequency effects, we calculated phase-locking spectra showing entrainment to frequencies between 1 and 100 Hz (1-Hz steps, ±1-Hz bins; *SI Appendix*) during sham trials (blue) and active tACS (orange). Solid lines and shaded error bars correspond to medians and IQRs (i.e., 25th and 75th percentiles). Stimulation was applied at 5 Hz (*Top*), 10 Hz, 20 Hz, and 40 Hz (*Bottom*) to the HC/BG target. In each condition, entrainment of HC/BG neurons only increased (horizontal black lines indicate differences significant at the $P < 0.01$ level) at or near the tACS frequency (black triangles). No other significant changes were observed. (*B*) Neurons outside the targeted area are not entrained at all. To test the spatial specificity of tACS, the same analysis was performed by using simultaneously recorded neurons from area TEO. No consistent entrainment was found for these cells in any condition or at any frequency. As TEO is a visual area, this result also corroborates the hypothesis that spike entrainment was caused by tACS rather than retinal stimulation. *SI Appendix*, Fig. S4 shows single-cell effects within TEO.

Fig. 4*B* compares the effectiveness of the two montages by subtracting the data from the stimulation and sham conditions. Here the red line indicates the change in PLV produced by the original montage (i.e., the difference between the orange and blue traces in Fig. 4, *Left*), whereas the green line indicates the changes produced by the mirrored montage. The original montages are significantly more effective ($P = 0.01$ and $P = 0.004$, Wilcoxon rank-sum tests) than the mirrored controls, demonstrating again the spatial specificity of tACS stimulation.

Entrainment Is Unlikely to Be Caused by Peripheral or Retinal Stimulation. The data in Fig. 4 also serve as an important control for phosphenes, a common side effect of tACS. During tACS,

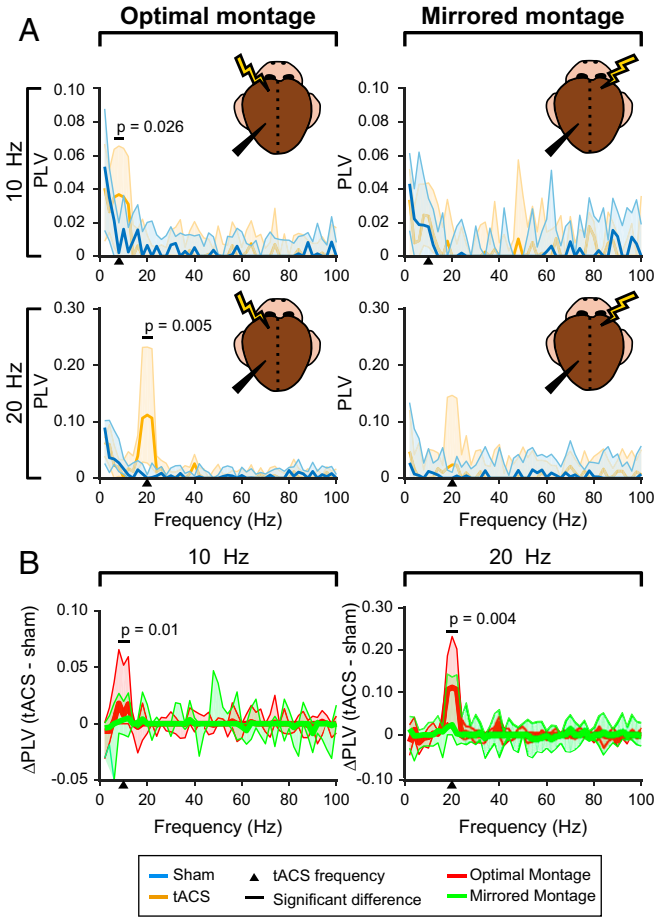

Fig. 4. Single-neuron entrainment is specific to the stimulation montage. (*A*) Phase-locking spectra, as in Fig. 3, for a montage optimized to stimulate the recording site (*Left*; see also *Inset*) and a mirror-image version applied over the contralateral hemisphere (*Right*). Stimulation was applied at 10 Hz (*Top*) and 20 Hz (*Bottom*). Data from sham (blue) and active tACS (orange) are shown for each montage, with solid lines and shaded error bars indicating the medians and IQRs (i.e., 25th and 75th percentiles), respectively. As in Fig. 3, stimulating via the optimal montage (Fp1 and O1) leads to significantly increased entrainment, indicated by the horizontal black bars, which is specific to the tACS frequency (black arrow). When the mirrored montage (Fp2 and O2) was used instead, no significant changes in entrainment were observed. (*B*) tACS produced significantly larger entrainment effects when applied through the optimal montage. To determine whether the differences in entrainment seen in *A* are themselves significant, we calculated the change in phase locking (tACS minus sham) produced by the optimal montage (red) vs. the mirrored montage (green). The data for 10-Hz (*Left*) and 20-Hz (*Right*) tACS are plotted in the same format as *A*. This analysis confirms that tACS is spatially specific (see also Fig. 3) and acts as control against peripheral nerve stimulation (*Results*).

some of the current applied to the head is shunted along the scalp and into the eyes, directly stimulating cells in the retina (50–52). This activity then propagates throughout posterior and temporal visual areas (53). Neurons in or downstream of these areas could, in principle, become entrained to this input rather than the electric field itself, and a similar technique has been shown to improve HC-dependent memory in humans (54, 55).

However, the mirrored montage experiments suggest that this pathway does not produce the entrainment effects shown in Figs. 1–3. The anterior–posterior positions of the stimulating electrodes determine the amount of shunting through the retina and therefore the strength of phosphene production (50). Montages matched in terms of anterior–posterior position should thus produce equivalent amounts of retinal stimulation. Furthermore, shunted current affects projections to both hemispheres via the temporal and nasal parts of the retina, even if applied unilaterally, as human observers report tACS-induced phosphenes in both hemifields (56). If our entrainment results were caused by visual input, we would therefore expect the optimized and mirrored montages to entrain neurons equally well. However, as Fig. 4 shows, we observed significantly less ($P < 0.01$)—and, in fact, zero—entrainment when the mirrored montages were applied. Additionally, a retinal influence would likely be strongest in visual areas (53), but recordings from TEO, a midlevel visual area, showed no entrainment when tACS was targeted at our sites in the deep brain (Fig. 3*B* and *SI Appendix*, Fig. S4).

Finally, perceptual data from humans receiving tACS under similar conditions also suggest that phosphenes and other peripheral effects are unlikely to produce the entrainment we see here. Phosphenes are a common side effect of stimulation at 10–20 Hz, but are absent or difficult to evoke at other frequencies (50, 56–58). However, we observed strong, statistically significant entrainment at 5 and 40 Hz, which is again inconsistent with a retinal origin.

Along with phosphenes, the onset of tACS can produce tactile sensations as a result of activation of somatosensory afferents in the scalp. These percepts allow human subjects to effectively discriminate between tACS and no-stimulation conditions (59). However, subjects rapidly adapt to them, and a properly designed sham stimulus can effectively blind human subjects to the stimulation condition without passing appreciable current into the brain (39–41). It is difficult to interrogate a monkey's subjective experience, but because of the close anatomical and perceptual similarities between monkeys and humans, their perception of tACS is likely comparable. We thus compared our active stimulation against a sham rather than a no-stimulation condition (*SI Appendix*, *SI Materials and Methods*). Furthermore, we did not analyze the first 30 seconds of each block, when these onset effects are likely to be strongest.

Taken together, the design of our experiments, the spatial and frequency specificity of the responses, and the correspondence with known biophysical mechanisms all suggest that entrainment is unlikely to be the result of phosphenes, tactile sensations, or other indirect effects.

Discussion

There has been considerable uncertainty about the potential effects of tES on the primate brain. Published results suggest a range of attitudes, from cautious optimism that it can effectively modulate brain and behavior (12) to skepticism that enough current enters the brain to have any effect at all (18). These assessments, however, are based on extrapolations, often from less realistic model systems, or indirect measures of neural activity. Here, we have presented data from nonhuman primates, a highly realistic model of the human brain, demonstrating that tACS reliably entrains the spiking activity of single neurons. This entrainment is limited to the frequency of stimulation and the vicinity of the targeted brain region.

Data from transcranial stimulation experiments are often difficult to interpret because of the numerous possible artifacts and confounds. Human experiments have purported to show that tACS entrains EEG oscillations, but there has been some skepticism regarding these results. In an EEG experiment, the stimulation artifact (e.g., 10-Hz tACS) and putative neural effect (change in 10-Hz oscillations) overlap precisely. Focusing on spiking activity, which has very different spectral content from the tACS waveform, allowed us to avoid this contamination. We were also able to exclude a potential influence of retinal stimulation, which has clouded the interpretation of previous work (50), by comparing two stimulation montages that would be expected to produce similar effects on the retina. These produced very different results on brain activity (Fig. 4), suggesting that our effects are not a result of retinal activation. Other sources of noise or indirect effects (e.g., tactile percepts, changes

in arousal) would also have relatively poor spatial specificity. However, we found that the influence of tACS was heterogeneous within a small volume of tissue (Fig. 1 *C* and *D*) and yet confined to the targeted region (Figs. 3*B* and 4).

In our previous work in nonhuman primates, we showed that tES using direct, rather than alternating, current alters synchrony between multiunit activity in one brain area and LFPs in another. However, we were unable to detect changes in single-unit spike rate or spike timing (21). Contemporary work by Kar et al. (23) also found that 10-Hz tACS altered neuronal adaptation to visual stimuli, but the authors were unable to measure single neuron responses during stimulation as a result of technical limitations. Although these results imply that tES can somehow affect the brain, they did not demonstrate that it ultimately changes spiking activity, which is widely regarded to be the primary means of coding and communication within the nervous system.

There has been some debate over the strength of the electric field reaching the brain and the field strengths necessary to produce neuronal effects. In our experiments, we modeled and measured field strengths of 0.2–0.3 V/m in the target area; these values are similar to—and, in some cases, slightly weaker than—those produced in human experiments (16, 17). The results from in vitro and small animal experiments at similar field strengths are mixed. In slices, Anastassiou et al. (60) found increased entrainment at 1 Hz, but not at 8 or 30 Hz, using a field of ∼0.75 V/m. Reato et al. (30), however, also found robust entrainment effects in slices exposed to 0.2-V/m fields, as did Chan and Nicholson (61) at 0.1–0.2 V/m. In a rodent model, Ozen et al. (15) argued that fields below 1 V/m had little effect, but some of their experiments with weaker fields also produced entrainment in as many as 33% of neurons (see figure 4 in ref. 15), similar to what we report here. These previous results can be reconciled with ours if one considers that we collected nearly an order of magnitude more spikes per neuron (∼15,000), which provided the statistical power needed to detect the sometimes-subtle entrainment effects shown in Fig. 2.

Our results also differ from those of Lafon et al. (24), who reported an unsuccessful attempt to entrain sleep spindles by applying low-frequency tACS in human subjects. However, the electric fields used in this study were quite weak (<<0.05 V/m) and, unlike single unit activity, sleep spindles are complex nonlocal phenomena generated by interactions between multiple brain regions (62). As such, stronger fields and novel, multifocal stimulation may be needed to entrain them. Consistent with this idea, Ketz et al. (63) recently described a closed-loop tACS approach during sleep that improves long-term memory consolidation in a target detection task by modulating endogenous slow-wave oscillations.

If the effects of tACS require 15,000 spikes to be detectable, are they too weak to influence behavior? Our data do not directly address this point, but the entrainment changes reported here, particularly during 20-Hz stimulation, are comparable to those linked with behavioral changes. Specifically, increases of ∼0.1 PLV have been associated with changes in sensory representations and working memory (64, 65), perceptual organization (2), behavioral state (66), learning and reward expectancy (67), and the retrieval of memories (68). Changes in synchronous activity appear to underlie momentary lapses in performance (4) and serious pathological conditions (5), so even small changes in spike timing, when distributed across a network of neurons, may exert a powerful influence on behavior. Moreover, optogenetic tools have allowed researchers to causally manipulate spike timing in laboratory animals with observable effects on behavior (69). Our results suggest that tACS may provide a way to noninvasively manipulate rhythmic activity in humans as well.

We focused on the HC and BG because they are appealing targets for translational research. Deep brain stimulation of the BG is already a routine treatment for several conditions, and there is some evidence for a role of invasive stimulation of the HC in memory enhancement (31). From a technical standpoint, the HC may be a particularly challenging test bed for neurostimulation because it has strong endogenous oscillations that generate their own electric fields (70). However, HC and BG do have the advantage of bordering a large ventricle, which allows for stimulation by current passing directly through the brain as well as current shunted through the highly conductive cerebrospinal fluid (71). It may be more difficult to produce fields as strong as these in other deep structures, especially with conventional tES techniques. Nevertheless, fields as high as 0.8 V/m, nearly four times stronger than the fields used here, have been produced by tES targeting the cortical surface (16, 17), so it should be possible to entrain neurons in those areas at least as well. As shown in Fig. 4, the montage must be chosen carefully to do so.

Grossman et al. (29) recently demonstrated that a novel form of tES using temporally interfering waveforms could be used to stimulate deep structures in the mouse brain. Although this and other advanced techniques may produce stronger and more focal stimulation, our data demonstrate that similar effects can be achieved by using conventional two-electrode tACS. This is true even in the primate, in which the HC is ∼30 mm below the skull surface, rather than ∼3 mm as it is in the mouse. The human tES literature has largely focused on cortical targets, but our results suggest that stimulation of deep structures may be surprisingly easy to achieve in humans as well.

One limitation of this work is that we could record single-unit activity from only a small subset of possible brain areas. Because the current passes through many areas as it travels between the stimulating electrodes, it remains possible that stimulation actually affected some other, unobserved area, which subsequently entrained neurons near our recording sites. We think many of the controls detailed here earlier mitigate against this possibility: entrainment effects were not found in brain regions near the target site, for which the identical argument could be advanced. Moreover, we observed that tACS altered bursting in single neurons. Although bursting can arise from network dynamics (72) or very specific sensory input (73), it is typically thought to reflect local, cell-intrinsic properties (42, 74), especially when the overall firing rate does not change, as we report here. Because subthreshold depolarizations are known to inhibit bursting (42, 75, 76), these results are thus consistent with a local effect whereby tACS causes small, subthreshold changes in neurons' membrane potentials. Ultimately, a full picture of the effects of tACS on brain activity will require simultaneous measurement of activity in many different brain regions with millisecond temporal resolution.

In conclusion, our data indicate that tACS entrains the activity of individual neurons in the primate brain. It does so in a spatially localized and frequency-specific manner that suggests that the electric fields produced during tACS directly affect neurons within the targeted area. Our data therefore provide a mechanistic rationale for applying tACS to human subjects and, more generally, suggest that other forms of tES may have direct neural effects as well.

Materials and Methods

Data for these experiments were collected from two adult male rhesus monkeys (*Macaca mulatta*) by using techniques very similar to those used in our previous study (21). All procedures described here were approved by the Animal Care Committee of the Montreal Neurological Institute and conformed to the guidelines of the Canadian Council on Animal Care. Full details of our task design, stimulation, neurophysiological recordings, and analysis are provided in the *SI Appendix*.

Note Added in Proof. Following the submission of our manuscript, Asamoah et al. (77) published a report suggesting that tACS affects cortical neurons via transcutaneous stimulation of peripheral nerves. Our data—especially those presented in Fig. 4—and the data in ref. 21 are difficult to reconcile with that hypothesis. However, it will be important in future work to identify a potential contribution of peripheral nerves, using methods comparable to those used here.

ACKNOWLEDGMENTS. We thank Julie Coursol, Cathy Hunt, and Dr. Fernando Chaurand for outstanding technical assistance. This work was supported by Defense Advanced Research Projects Agency Contract N66001-16-C-4058 (Memory Enhancement by Modulation of Encoding Strength; to P.K.P. and C.C.P.) and Canadian Institutes of Health Research Grant MOP-115178 (to C.C.P.). The views, opinions, and/or findings expressed are those of the authors and should not be interpreted as representing the official views or policies of the Department of Defense or the US Government.

1. O'Keefe J, Recce ML (1993) Phase relationship between hippocampal place units and the EEG theta rhythm. *Hippocampus* 3:317–330.
2. Vinck M, et al. (2010) Gamma-phase shifting in awake monkey visual cortex. *J Neurosci* 30:1250–1257.
3. Fries P (2015) Rhythms for cognition: Communication through coherence. *Neuron* 88:220–235.
4. Rutishauser U, Ross IB, Mamelak AN, Schuman EM (2010) Human memory strength is predicted by theta-frequency phase-locking of single neurons. *Nature* 464:903–907.
5. Spencer KM, et al. (2004) Neural synchrony indexes disordered perception and cognition in schizophrenia. *Proc Natl Acad Sci USA* 101:17288–17293.
6. Kirov R, Weiss C, Siebner HR, Born J, Marshall L (2009) Slow oscillation electrical brain stimulation during waking promotes EEG theta activity and memory encoding. *Proc Natl Acad Sci USA* 106:15460–15465.
7. Marshall L, Mölle M, Hallschmid M, Born J (2004) Transcranial direct current stimulation during sleep improves declarative memory. *J Neurosci* 24:9985–9992.
8. Kallel L, Mondino M, Brunelin J (2016) Effects of theta-rhythm transcranial alternating current stimulation (4.5 Hz-tACS) in patients with clozapine-resistant negative symptoms of schizophrenia: A case series. *J Neural Transm (Vienna)* 123:1213–1217.
9. Horvath JC, Forte JD, Carter O (2015) Evidence that transcranial direct current stimulation (tDCS) generates little-to-no reliable neurophysiologic effect beyond MEP amplitude modulation in healthy human subjects: A systematic review. *Neuropsychologia* 66:213–236.
10. Horvath JC, Forte JD, Carter O (2015) Quantitative review finds no evidence of cognitive effects in healthy populations from single-session transcranial direct current stimulation (tDCS). *Brain Stimul* 8:535–550.
11. Dedoncker J, Brunoni AR, Baeken C, Vanderhasselt MA (2016) A systematic review and meta-analysis of the effects of transcranial direct current stimulation (tDCS) over the dorsolateral prefrontal cortex in healthy and neuropsychiatric samples: Influence of stimulation parameters. *Brain Stimul* 9:501–517.
12. Berryhill ME, Martin D (2018) Cognitive effects of transcranial direct current stimulation in healthy and clinical populations: An overview. *J ECT* 34:e25–e35.
13. Terzuolo CA, Bullock TH (1956) Measurement of imposed voltage gradient adequate to modulate neuronal firing. *Proc Natl Acad Sci USA* 42:687–694.
14. Francis JT, Gluckman BJ, Schiff SJ (2003) Sensitivity of neurons to weak electric fields. *J Neurosci* 23:7255–7261.
15. Ozen S, et al. (2010) Transcranial electric stimulation entrains cortical neuronal populations in rats. *J Neurosci* 30:11476–11485.
16. Huang Y, et al. (2017) Measurements and models of electric fields in the *in vivo* human brain during transcranial electric stimulation. *eLife* 6:e18834.
17. Opitz A, et al. (2016) Spatiotemporal structure of intracranial electric fields induced by transcranial electric stimulation in humans and nonhuman primates. *Sci Rep* 6:31236.
18. Vöröslakos M, et al. (2018) Direct effects of transcranial electric stimulation on brain circuits in rats and humans. *Nat Commun* 9:483.
19. Schambra HM, Bikson M, Wager TD, DosSantos MF, DaSilva AF (2014) It's all in your head: Reinforcing the placebo response with tDCS. *Brain Stimul* 7:623–624.
20. Sadleir RJ, Vannorsdall TD, Schretlen DJ, Gordon B (2010) Transcranial direct current stimulation (tDCS) in a realistic head model. *Neuroimage* 51:1310–1318.
21. Krause MR, et al. (2017) Transcranial direct current stimulation facilitates associative learning and alters functional connectivity in the primate brain. *Curr Biol* 27:3086–3096.e3.
22. Toleikis JR, Sances A, Jr, Larson SJ (1974) Effects of diffuse transcerebral electrical currents on cortical unit potential activity. *Anesth Analg* 53:48–55.
23. Kar K, Duijnhouwer J, Krekelberg B (2017) Transcranial alternating current stimulation attenuates neuronal adaptation. *J Neurosci* 37:2325–2335.
24. Lafon B, et al. (2017) Low frequency transcranial electrical stimulation does not entrain sleep rhythms measured by human intracranial recordings. *Nat Commun* 8:1199.
25. Bikson M, et al. (2004) Effects of uniform extracellular DC electric fields on excitability in rat hippocampal slices in vitro. *J Physiol* 557:175–190.
26. Radman T, Ramos RL, Brumberg JC, Bikson M (2009) Role of cortical cell type and morphology in subthreshold and suprathreshold uniform electric field stimulation in vitro. *Brain Stimul* 2:215–228.e1-3.
27. Radman T, Su Y, An JH, Parra LC, Bikson M (2007) Spike timing amplifies the effect of electric fields on neurons: Implications for endogenous field effects. *J Neurosci* 27: 3030–3036.
28. Anastassiou CA, Montgomery SM, Barahona M, Buzsáki G, Koch C (2010) The effect of spatially inhomogeneous extracellular electric fields on neurons. *J Neurosci* 30:1925–1936.
29. Grossman N, et al. (2017) Noninvasive deep brain stimulation via temporally interfering electric fields. *Cell* 169:1029–1041.e16.
30. Reato D, Rahman A, Bikson M, Parra LC (2010) Low-intensity electrical stimulation affects network dynamics by modulating population rate and spike timing. *J Neurosci* 30:15067–15079.
31. Hampson RE, et al. (2018) Developing a hippocampal neural prosthetic to facilitate human memory encoding and recall. *J Neural Eng* 15:036014.
32. Titiz AS, et al. (2017) Theta-burst microstimulation in the human entorhinal area improves memory specificity. *eLife* 6:e29515.
33. Miller JP, et al. (2015) Visual-spatial memory may be enhanced with theta burst deep brain stimulation of the fornix: A preliminary investigation with four cases. *Brain* 138:1833–1842.
34. Ramayya AG, Misra A, Baltuch GH, Kahana MJ (2014) Microstimulation of the human substantia nigra alters reinforcement learning. *J Neurosci* 34:6887–6895.
35. Suthana N, et al. (2012) Memory enhancement and deep-brain stimulation of the entorhinal area. *N Engl J Med* 366:502–510.
36. Perlmutter JS, Mink JW (2006) Deep brain stimulation. *Annu Rev Neurosci* 29:229–257.
37. DeLong MR, Wichmann T (2015) Basal Ganglia circuits as targets for neuromodulation in Parkinson disease. *JAMA Neurol* 72:1354–1360.
38. Datta A, et al. (2016) On comparing in vivo intracranial recordings in non-human primates to predictions of optimized transcranial electrical stimulation. *Conf Proc IEEE Eng Med Biol Soc* 2016:1774–1777.
39. Wach C, et al. (2013) Effects of 10 Hz and 20 Hz transcranial alternating current stimulation (tACS) on motor functions and motor cortical excitability. *Behav Brain Res* 241:1–6.
40. Jaušovec N, Jaušovec K, Pahor A (2014) The influence of theta transcranial alternating current stimulation (tACS) on working memory storage and processing functions. *Acta Psychol (Amst)* 146:1–6.
41. Hoy KE, et al. (2015) The effect of γ-tACS on working memory performance in healthy controls. *Brain Cogn* 101:51–56.
42. Wang Z, McCormick DA (1993) Control of firing mode of corticotectal and corticopontine layer V burst-generating neurons by norepinephrine, acetylcholine, and 1S,3R-ACPD. *J Neurosci* 13:2199–2216.
43. Liu A, et al. (2018) Immediate neurophysiological effects of transcranial electrical stimulation. *Nat Commun* 9:5092.
44. Mitchell JF, Sundberg KA, Reynolds JH (2007) Differential attention-dependent response modulation across cell classes in macaque visual area V4. *Neuron* 55:131–141.
45. Mikula S, Trotts I, Stone JM, Jones EG (2007) Internet-enabled high-resolution brain mapping and virtual microscopy. *Neuroimage* 35:9–15.
46. Seress L (1978) Pyramid-like basket cells in the granular layer of the dentate gyrus in the rat. *J Anat* 127:163–168.
47. Buckmaster PS, Amaral DG (2001) Intracellular recording and labeling of mossy cells and proximal CA3 pyramidal cells in macaque monkeys. *J Comp Neurol* 430:264–281.
48. Buckmaster PS, Alonso A, Canfield DR, Amaral DG (2004) Dendritic morphology, local circuitry, and intrinsic electrophysiology of principal neurons in the entorhinal cortex of macaque monkeys. *J Comp Neurol* 470:317–329.
49. Okun M, et al. (2015) Diverse coupling of neurons to populations in sensory cortex. *Nature* 521:511–515.
50. Kar K, Krekelberg B (2012) Transcranial electrical stimulation over visual cortex evokes phosphenes with a retinal origin. *J Neurophysiol* 108:2173–2178.
51. Schutter DJ, Hortensius R (2010) Retinal origin of phosphenes to transcranial alternating current stimulation. *Clin Neurophysiol* 121:1080–1084.
52. Schwiedrzik CM (2009) Retina or visual cortex? The site of phosphene induction by transcranial alternating current stimulation. *Front Integr Nuerosci* 3:6.
53. Taylor PC, Walsh V, Eimer M (2010) The neural signature of phosphene perception. *Hum Brain Mapp* 31:1408–1417.
54. Williams JH (2001) Frequency-specific effects of flicker on recognition memory. *Neuroscience* 104:283–286.
55. Williams J, Ramaswamy D, Oulhaj A (2006) 10 Hz flicker improves recognition memory in older people. *BMC Neurosci* 7:21.
56. Kanai R, Chaieb L, Antal A, Walsh V, Paulus W (2008) Frequency-dependent electrical stimulation of the visual cortex. *Curr Biol* 18:1839–1843.
57. Lorenz R, et al. (2017) Assessing tACS-induced phosphene perception using closed-loop Bayesian optimization. bioRxiv:10.1101/150086. Preprint, posted June 14, 2017.
58. Motokawa K, Ebe M (1952) Selective stimulation of color receptors with alternating currents. *Science* 116:92–94.
59. Turi Z, et al. (2013) Both the cutaneous sensation and phosphene perception are modulated in a frequency-specific manner during transcranial alternating current stimulation. *Restor Neurol Neurosci* 31:275–285.
60. Anastassiou CA, Perin R, Markram H, Koch C (2011) Ephaptic coupling of cortical neurons. *Nat Neurosci* 14:217–223.
61. Chan CY, Nicholson C (1986) Modulation by applied electric fields of Purkinje and stellate cell activity in the isolated turtle cerebellum. *J Physiol* 371:89–114.
62. Amzica F, Steriade M (2000) Integration of low-frequency sleep oscillations in corticothalamic networks. *Acta Neurobiol Exp (Warsz)* 60:229–245.
63. Ketz N, Jones AP, Bryant NB, Clark VP, Pilly PK (2018) Closed-loop slow-wave tACS improves sleep dependent long-term memory generalization by modulating endogenous oscillations. *J Neurosci* 38:7314–7326.
64. Bahmani Z, Daliri MR, Merrikhi Y, Clark K, Noudoost B (2018) Working memory enhances cortical representations via spatially specific coordination of spike times. *Neuron* 97:967–979.e6.
65. van Wingerden M, Vinck M, Lankelma JV, Pennartz CM (2010) Learning-associated gamma-band phase-locking of action-outcome selective neurons in orbitofrontal cortex. *J Neurosci* 30:10025–10038.
66. Vinck M, et al. (2016) Cell-type and state-dependent synchronization among rodent somatosensory, visual, perirhinal cortex, and Hippocampus CA1. *Front Syst Neurosci* 9:187.
67. van Wingerden M, Vinck M, Lankelma J, Pennartz CM (2010) Theta-band phase locking of orbitofrontal neurons during reward expectancy. *J Neurosci* 30:7078–7087.
68. Foster BL, Kaveh A, Dastjerdi M, Miller KJ, Parvizi J (2013) Human retrosplenial cortex displays transient theta phase locking with medial temporal cortex prior to activation during autobiographical memory retrieval. *J Neurosci* 33:10439–10446.
69. Siegle JH, Pritchett DL, Moore CI (2014) Gamma-range synchronization of fast-spiking interneurons can enhance detection of tactile stimuli. *Nat Neurosci* 17:1371–1379.

70. Qiu C, Shivacharan RS, Zhang M, Durand DM (2015) Can neural activity propagate by endogenous electrical field? *J Neurosci* 35:15800–15811.
71. Huang Y, Parra LC (2018) Can transcranial electric stimulation with multiple electrodes reach deep targets? bioRxiv:10.1101/382598. Preprint, posted August 1, 2018.
72. Fee MS, Kozhevnikov AA, Hahnloser RH (2004) Neural mechanisms of vocal sequence generation in the songbird. *Ann N Y Acad Sci* 1016:153–170.
73. Neiman AB, Russell DF (2002) Synchronization of noise-induced bursts in noncoupled sensory neurons. *Phys Rev Lett* 88:138103.
74. Llinás RR, Steriade M (2006) Bursting of thalamic neurons and states of vigilance. *J Neurophysiol* 95:3297–3308.
75. Schwindt P, Crill W (1999) Mechanisms underlying burst and regular spiking evoked by dendritic depolarization in layer 5 cortical pyramidal neurons. *J Neurophysiol* 81: 1341–1354.
76. Jensen MS, Azouz R, Yaari Y (1996) Spike after-depolarization and burst generation in adult rat hippocampal CA1 pyramidal cells. *J Physiol* 492:199–210.
77. Asamoah B, Khatoun A, Mc Laughlin M (2019) tACS motor system effects can be caused by transcutaneous stimulation of peripheral nerves. *Nat Commun* 10:266.

PNAS
www.pnas.org

Supplementary Information for

Transcranial alternating current stimulation entrains single-neuron activity in the primate brain

Matthew R. Krause[*1], Pedro G. Vieira[*1], Bennett A. Csorba[1], Praveen K. Pilly[2], Christopher C. Pack[1§]

[1] Montreal Neurological Institute, McGill University, Montreal, QC H3A 2B4, Canada
[2] Information and Systems Sciences Laboratory, HRL Laboratories, LLC, Malibu, CA 90265, USA
* These authors contributed equally

Corresponding author:
Christopher C. Pack
christopher.pack@mcgill.ca

This PDF file includes:

www.pnas.org/cgi/doi/10.1073/pnas.1815958116

SI Materials and Methods

Data for these experiments were collected from two adult male rhesus monkeys (*macaca mulatta*), using techniques very similar to those used in our previous study (1). Monkey F (6 years, 14 kg) participated in both studies, while monkey N (5 years, 7.5 kg) was obtained for these experiments. However, with the exception of the finite-element modeling for Monkey F, none of these data have been published previously.

All procedures described here were approved by the Animal Care Committee of the Montreal Neurological Institute and conformed to the guidelines of the Canadian Council on Animal Care. Since the experiments described in this paper use a within-cell design, no specific group assignments were needed; conditions were pseudo-randomly interleaved and separated by a 5-minute inter-stimulus interval to avoid possible carryover effects. Linear mixed-effects models, with a fixed effect of stimulation and random effect of block, were used to assess firing rates for individual neurons. Elsewhere, we used non-parametric tests throughout, which make no distributional assumptions about the data.

Animal Preparation

We began by acquiring high-resolution T_1 and T_2-weighted MRIs of each animal's head and neck with a Siemens 3T Trio scanner. An MP-RAGE pulse sequence was used for the T_1 scans (TR = 2300 ms and TE = 3.59ms); the T_2-weighted images used a TR = 2800 ms and TE = 489ms instead. Between 7 and 10 separate volumes with 0.6mm isotropic voxels were acquired using each pulse sequence. Volumes were denoised, aligned, and averaged with FSL and AFNI. These scans were used to optimize the tACS stimulation (below).

A sterile surgical procedure was performed to attach a titanium head holder (Hybex Innovations, Montreal) to the animals' skulls. Animals were allowed to recover for eight weeks, and then familiarized with the laboratory environment, head restraint, and the fixation task. Next, the animals were prepared for neurophysiological recording. We attached MR-opaque fiducially markers (Rogue Research, Montreal) to the head holder and acquired a second set of T_1-weighted images for surgical planning. Using a neuronavigation system with millimeter precision (BrainSight Vet, Rogue Research), we targeted three sites: the right ventrolateral prefrontal cortex (PFC, areas 9/46v) and left posterior inferotemporal cortex (TEO) on the cortical surface and banks of the lateral ventricle deep in the brain.

Iridium oxide Utah arrays (Blackrock Microsystems) were implanted in the two superficial brain areas. In Monkey F, two separate 96-channel arrays, each with their own connector, were implanted in PFC and TEO. Since monkey N had a smaller head, two 64-channel arrays, attached to a single "MultiPort" connector, were used instead. All electrodes were 1.5mm long and placed in a square grid, with 400 µm separation between electrodes in each direction. Target locations were verified based on the sulcal patterns and neuronavigation data.

We also implanted a recording cylinder to permit daily-acute recordings from deep brain structures; trajectories were planned using neuronavigation software. To verify recording sites for deep brain locations, a post-operative CT scan was performed. Stainless steel guide tubes were inserted into the recording chamber and a 250µm tungsten electrode (FHC) was inserted into the brain and moved to a position 5mm above the targeted location (Supplementary Figure 1). We acquired a single volume with 150 µm isotropic voxels using a Vimago CT scanner (90 kVp).

Behavioral Task

Arousal, motivational state, and oculomotor activity strongly affect rhythmic brain activity. We used a simple fixation task to minimize eye movements and to ensure that animals remained in a consistent behavioral state throughout the experiment. This approach also allowed us to collect more spikes per neuron than would be possible in a more complex behavioral paradigm. Animals sat in a standard primate chair (Crist Instruments), placed 57 cm from a computer monitor that covered the central 30˚ x 60˚ of the visual field, while their eye position was monitored with an infrared eye tracker (SR Research, Ontario). The monkeys were trained to fixate a small black target (0.5˚) presented against a neutral grey background (54 cd/m^2). Liquid rewards were dispensed whenever their gaze remained within 1-2˚ of the fixation target for ~1-2 seconds: the exact delays were drawn from an exponential distribution to prevent entrainment to rewards or expected rewards. Custom software written in Matlab (The Mathworks, Natick, MA, USA) controlled the behavioral task and coordinated the eye tracker, tES stimulator, and recording hardware.

Transcranial Electrical Stimulation

Individualized finite-element models (FEM) were used to optimize the tES electrode montages for each animal using the approach described in Datta et al. (2). To build the models, the initial T1 and T2-weighted scans were segmented into five tissue types (grey matter, white matter, cerebrospinal fluid, bone, and skin). The model was then updated with the position and composition of all transcranial and intracranial implants, using positions recorded during the surgeries. The FEM was solved to find an electrode montage that maximized the field strength along the inferior horn of the lateral ventricle while avoiding the devices implanted in the skull. This provided access to sites that are frequently used in brain stimulation studies, including the hippocampus and basal ganglia. Within the latter structure, our fMRI and CT imaging suggest that most recordings came from the substantia nigra (Figure S1), although this was not verified histologically. Although the electric fields can be made arbitrarily strong by increasing the current, most human studies limit the stimulation current to 1-2 mA to reduce user discomfort and tissue heating. While recent studies have shown that higher currents may be tolerable, we limited our montages to a total of ±2 mA so that the data would be directly comparable with human experiments. In 10-20 coordinates, the optimal electrode locations were F3 and O2 for Monkey F, and FP1 and O1 for Monkey N.

Several recent papers have validated this modeling approach (3-7). Nevertheless, we measured the field strength in both animals via robust linear regression. The field, in the direction of our electrode, was defined as the slope of the tACS artifact amplitude vs. electrode position line. In monkey N, several recording sites clearly had several components with different slopes. To address this, we fit piecewise linear models with 2 and 3 components, and used the steepest slope from the best fitting model as the field strength.

We applied tACS using an unmodified StarStim8 system (Neuroelectrics, Cambridge MA), which is marketed for human use. We coated 1 cm (radius) Ag/AgCl electrodes (PISTIM; Neuroelectrics) with a conductive gel (SignaGel) and attached them to the intact scalp using a thin layer of silicon elastomer (Kwik-Sil, World Precision

Instruments). The impedance of the tACS electrodes was monitored throughout the experiment and was typically 1-2 kΩ and always below 10 kΩ.

While animals performed the fixation task, we applied active and sham tACS in randomly interleaved five-minute blocks. The stimulation waveform was a sinusoid of the specified frequency (here 5, 10, 20, or 40 cycles per second) with a peak amplitude of ±2 mA (4 mA peak-to-peak) and updated at 1000 Hz. At the beginning of each block, the amplitude was linearly ramped up from 0 to ±2 mA over 10 seconds. The full ±2 mA current was then applied for 5 minutes, after which the current was ramped back down from ±2 mA to zero over 10 seconds. Blocks were separated by a five-minute inter-trial interval, during which the monkey continued to perform the fixation task.

Shunted tACS current could potentially stimulate peripheral fibers in the skin, causing an itching sensation. These percepts could affect the animals' arousal levels and, thus, their neural activity. To minimize this confound, we compared data acquired during active tACS with data collected during sham blocks, not the inter-trial intervals. In a sham block, as in the active blocks described above, the current ramped up from 0 to ±2 mA, over 10 seconds. However, it only remained at full power for 10 seconds before ramping back down to zero. Current was also ramped up and down at the end of each block in a similar manner. Human subjects are generally unable to distinguish between these two protocols (8-10), so that the sham condition provides a valuable control for non-specific arousal or peripheral effects of stimulation. Consistent with this, animals sometimes reacted to the onset of stimulation in both conditions, but then rapidly calmed down, suggesting that the sham effectively mimics the sensations evoked by tACS. Since this sometimes produced motion artifacts or fixation breaks, we excluded the first and last 30 seconds of each block from analysis.

Neural Data Collection

Single-neuron data were obtained from the basal ganglia, hippocampus, and inferotemporal cortex. For both animals, the Utah arrays in PFC were no longer able to resolve single units by the time these experiments began, so no data from these arrays are available or shown here. At the beginning of each recording session, the dura inside the recording chamber was penetrated with a sharpened 22 ga. stainless steel guide tube. Next, a 32-channel V-Probe (Plexon Inc; 150 μm spacing) was inserted through the guide tube, and slowly lowered into the brain using a microdrive (Nan Instruments). The target depth and position were determined from each animal's MRI and CT scans. We simultaneously recorded wideband signals from the V-Probe and chronically implanted arrays using a Ripple Neural Interface Processor (Ripple Neuro). When artifacts from tACS approached the limits of our amplifiers (±6.8 mV), the recordings were referenced against a low-impedance channel on each electrode array. Otherwise, signals were referenced against the guide tube or the built-in reference wires (Utah arrays). The signal was bandpass filtered between 0.3-7500 Hz, sampled at 30,000 Hz, and stored at 16 bit and 0.21 μV resolution for offline analysis.

A PCA-based filtering algorithm, adapted from Helfrich et al. (11), was used to attenuate the tACS artifacts and manually reviewed for quality. Since this approach may not completely remove the stimulation artifacts (12), our results focus on single-unit activity, which is not affected by incomplete removal of the tACS artifacts. Single units were identified by bandpass filtering the signal (500-7000 Hz, 3rd order Butterworth filter), thresholding it at ±3 standard deviations (robustly estimated from the median absolute deviation), and extracting 2 ms intervals around each threshold crossing. The

segments were then clustered using UltraMegaSort 2000, a *k*-means over-clustering spike sorter (13). The clusters were then manually reviewed and refined. Several metrics were used to verify each putative single neuron, including: (1) good clustering of principal components scores, (2) stability of spike amplitude and width and (3) clear refractory period.

We were particularly concerned about artifacts generated during data acquisition or signal processing that could produce spike timing effects. These could occur for example if stimulation artifacts saturated the recording system, rendering us unable to detect spikes during certain phases of the tACS waveform (e.g., the peak or trough). To check for systematic clipping of our data, we computed the 0.01 and 99.9th percentiles of the wideband signals. The medians of these values were -4.3 mV, or 12,274 analog-to-digital units (ADU) and +4.2 mV (52,824 ADU), respectively, which is much smaller than our amplifier's dynamic range (±6.8 mV, 0-65,535 ADU). The cell with the largest wideband range still had more than 300 ADUs of headroom, and yet was not one of the most strongly affected cells (ΔPLV = 0.16 for 10 Hz tACS).

Data analysis

We quantified the neurons' phase locking to the electrical stimulation using pairwise phase consistency (PPC), a measure of the synchronization between a point process (spikes) and a continuous one (the tACS waveform), which has several statistical advantages over directly computing the phase-locking values (14). Separate PPC values were calculated for each neuron, using the spike times identified by the sorting procedure above and the wideband signal from an adjacent channel. Using an adjacent channel allows us to avoid spurious phase locking due to spike contamination of the local field potential (15), while remaining close enough to minimize any non-linear distortion of the tACS signal by physiological processes (12, 16). The wideband signal was downsampled to 1,000 Hz and bandpass filtered within ±1 Hz (3rd order, Butterworth filter) of frequency of interest (usually the tACS waveform, but see Figure 3). The signal's phase was calculated using the Hilbert transform. Phases at the time of each spike were extracted, and used to calculate the PPC. Data from sham trials were bandpass filtered to extract the same frequencies used in the tACS waveform (e.g., 10±1 Hz when compared against 10 Hz tACS) and processed in the same way.

Since neurons phase-lock to endogenous oscillations (17), it is not sufficient to merely test the distribution of spike phases for uniformity. Instead, we used a permutation test to compare PPC values across conditions. First, PPC values were calculated separately for each condition and subtracted. Next, phase values from both conditions were combined and two surrogate datasets, matching the sizes of the originals, were randomly drawn from the pooled data. PPC values were computed for each surrogate data set, then subtracted to find their difference. This process was repeated 1000 times to construct a null distribution. We then calculated the p-value by finding the number of surrogate datasets where the magnitude of the difference was at least as large as the magnitude of the true differences. The raw PPC values are difficult to interpret, so we rescaled them into an unbiased phase-locking value (PLV) by taking the square root of each PPC statistic. This facilitates comparisons with previous work, which has largely used PLVs (see Discussion).

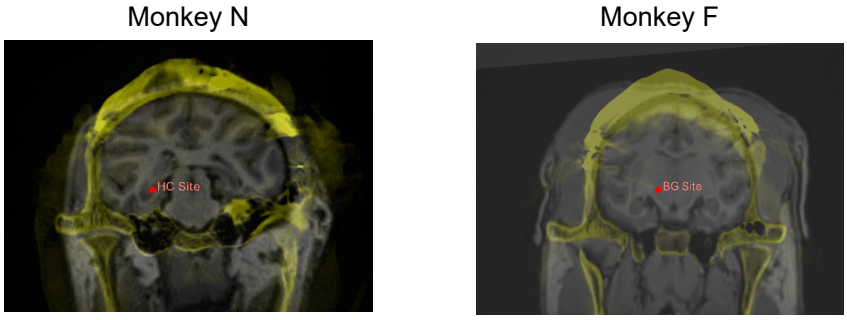

Fig. S1. Recording Sites. Post-operative CT scans showing typical recording sites in the hippocampus (left, monkey N) and basal ganglia (right, monkey F). To verify these locations, stainless steel guide tubes were inserted into the recording chamber and a 250µm tungsten electrode was inserted into the brain. Red dots indicate the recording positions. To avoid imaging artifacts, electrodes were slightly retracted before these scans were acquired.

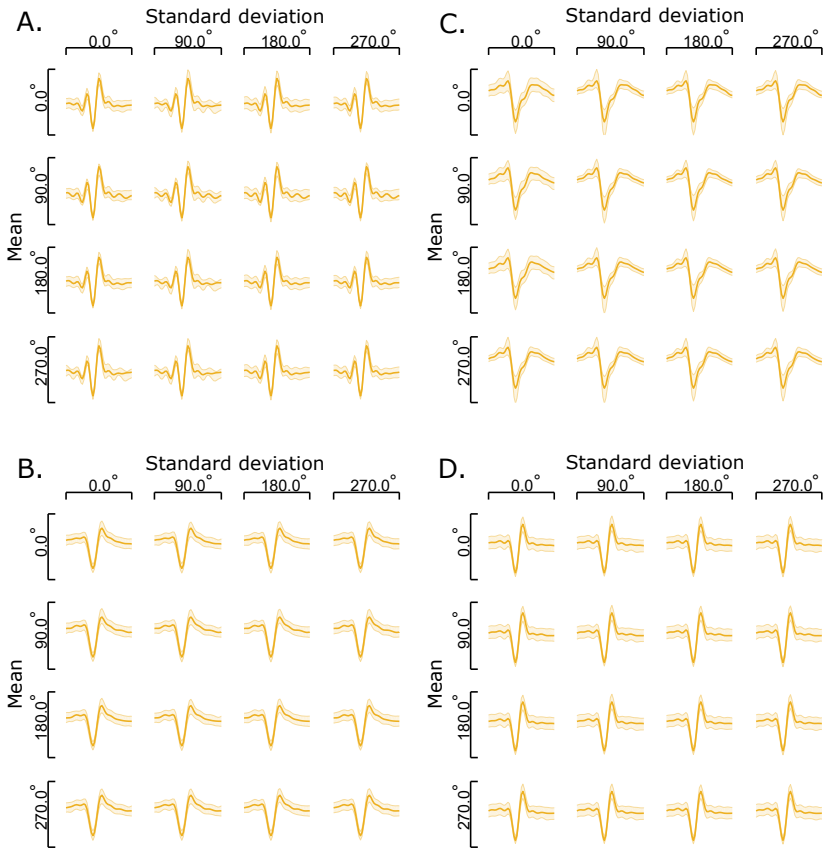

Fig. S2. Waveforms Do Not Change Across tACS Phases. For the neurons shown in Main Figure 1, spike waveforms were binned according to the phase of the tACS stimulation. Mean and standard deviations were calculated for each bin. As in Main Figure 1 (column 4), the means of one condition (here phase) were superimposed on the standard deviations of the others. No appreciable differences can be detected, indicating that spike shape—and thus detectability—remains constant during different phases of stimulation. See also Main Figure 1, where data from the same four neurons is shown.

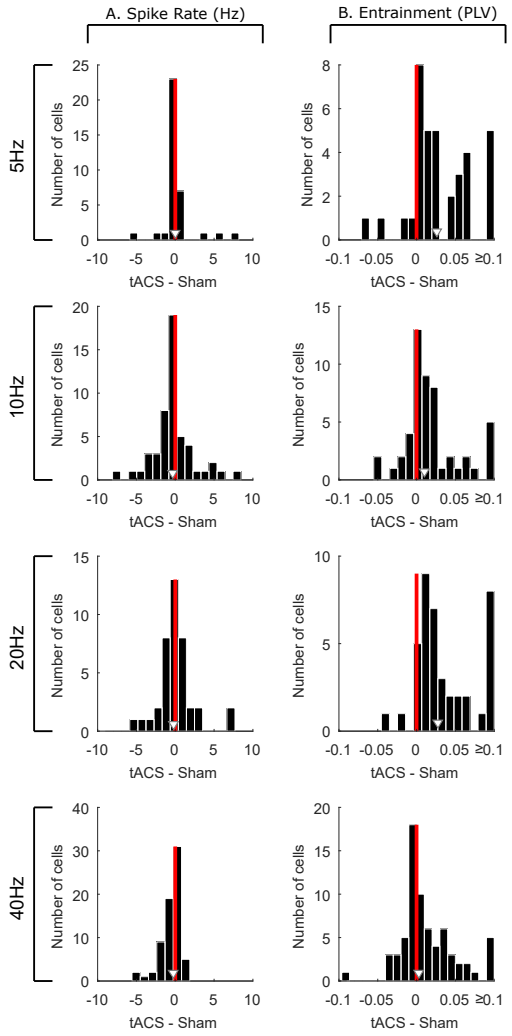

Fig S3. Population Effects of tACS on Firing Rate and Phase Locking Values. **(A)** Histograms showing the difference of firing rates values obtained from active tACS and sham conditions (tACS – sham) for each cell. Values are distributed around zero, indicating a small effect of tACS on firing rate. Red lines indicate zero, and the white triangles indicates the medians of each distribution. **(B)** Same as in A, but for changes in phase locking values (ΔPLV). ΔPLV values are significantly shifted towards positive values (see Main Text), indicating an entrainment of single unit activity by active tACS. See also Main Figure 2 for single-cell data.

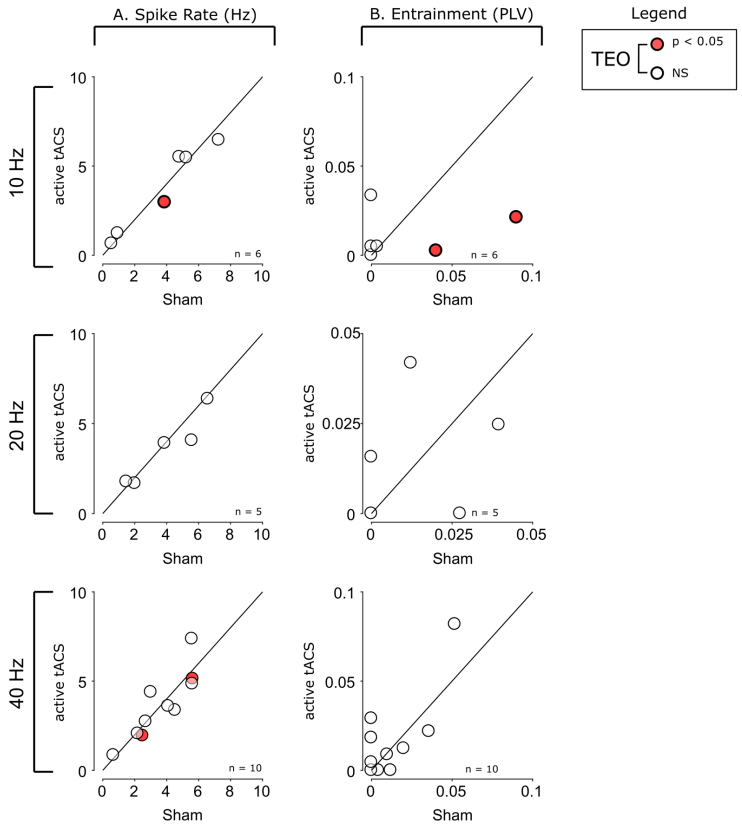

Fig S4. Population Distributions of Firing Rates and Phase Locking Values Obtained for TEO Cells. (A) Distributions of average firing rate during 10 Hz, 20 Hz and 40 Hz tACS. Firing rate values tend to fall along the equality line, indicating similar firing rates between conditions. Statistical significance is indicated by white (non-significant; $p \geq 0.05$) or red (significant; $p < 0.05$) colors. (B) Same as in A, but for phase locking values (PLV). No robust trends were detected for PLV during stimulation, indicating that tACS effects were specific to the targeted area. Note however that two cells show significantly decreased phase locking during 10 Hz tACS. See Main Figure 3 for population data.

Table S1. Central tendencies for firing rate, phase locking values, and circular variance split according to tACS frequency and brain area. Values are medians together with 25th and 75th percentiles as a measure of dispersion. * indicates $p < 0.05$; ** indicates $p < 0.01$. These data are depicted in Main Figure 2 and Supplemental Figure 4.

		BG		HC		TEO	
		SHAM	tACS	SHAM	tACS	SHAM	tACS
Firing Rate	5 Hz	0.6 [0.5 – 1.6]	0.8 [0.5 – 1.5]	11.6 [6.8 – 22.0]	10.8 [7.5 – 24.4]	–	–
	10 Hz	8.5 [4.9 – 17.6]	6.6 [3.9 – 17.7]	7.0 [3.5 – 22.7]	7.6 [3.8 – 22.4]	4.3 [0.9 – 5.2]	4.2 [1.2 – 5.5]
	20 Hz	10.6 [6.5 – 20.5]	11.0 [6.6 – 20.9]	10.2 [6.6 – 24.4]	9.6 [5.9 – 22.1]	3.9 [1.9 – 5.8]	3.9 [1.7 – 4.6]
	40 Hz	10.7 [5.9 – 16.6]	10.9 [5.1 – 15.1]	5.8 [2.3 – 8.2]	4.5 [2.3 – 7.5]	3.6 [2.5 – 5.6]	3.5 [2.1 – 4.8]
Phase Locking Value	5 HZ	0.006 [0 – 0.02]	0.035 * [0 – 0.08]	0.008 [0 – 0.02]	0.04 ** [0.01 – 0.05]	–	–
	10 Hz	0.008 [0 – 0.015]	0.022 ** [0.013 – 0.034]	0.016 [0 – 0.036]	0.035 * [0 – 0.064]	0 [0 – 0.09]	0.0012 [0 – 0.034]
	20 Hz	0 [0 – 0.009]	0.024 ** [0.018 – 0.039]	0 [0 – 0.062]	0.11 ** [0.03 – 0.23]	0.012 [0- 0.04]	0.015 [0 – 0.042]
	40 Hz	0.011 [0.005 – 0.016]	0.015 [0.01 – 0.026]	0.0019 [0 – 0.018]	0.038 ** [0.008 – 0.064]	0.007 [0 – 0.029]	0.010 [0 – 0.029]
Circular Variance	5 HZ	0.96 [0.91 – 0.97]	0.92 * [0.91 – 0.96]	0.98 [0.97 – 0.99]	0.96 ** [0.93 – 0.98]	–	–
	10 Hz	0.98 [0.96 – 0.99]	0.97 * [0.96 – 0.98]	0.97 [0.96 – 0.99]	0.95 * [0.92 – 0.97]	0.97 [0.96 – 0.98]	0.98 [0.96 – 0.98]
	20 Hz	0.99 [0.98 – 0.99]	0.97 ** [0.95 – 0.98]	0.99 [0.98 – 0.99]	0.88 ** [0.78 – 0.96]	0.97 [0.96 – 0.98]	0.98 [0.97 – 0.98]
	40 Hz	0.98 [0.97 – 0.99]	0.98 [0.95 – 0.98]	0.99 [0.97 – 0.99]	0.96 ** [0.93 – 0.97]	0.98 [0.96 – 0.98]	0.98 [0.98 – 0.99]

References

1. Krause MR*, et al.* (2017) Transcranial Direct Current Stimulation Facilitates Associative Learning and Alters Functional Connectivity in the Primate Brain. *Curr Biol* 27(20):3086-3096 e3083.
2. Datta A, Krause, M.R., Pilly, P.K., Choe, J., Zanos, T.P., Thomas, C., and Pack, C.C. (2016) On comparing in vivo intracranial recordings in non-human primates to predictions of optimized transcranial electrical stimulation. *Proceedings of the 38th Annual International Conference of the IEEE Engineering in Medicine and Biology Society*.
3. Kar K, Duijnhouwer J, & Krekelberg B (2017) Transcranial Alternating Current Stimulation Attenuates Neuronal Adaptation. *J Neurosci* 37(9):2325-2335.
4. Lafon B*, et al.* (2017) Low frequency transcranial electrical stimulation does not entrain sleep rhythms measured by human intracranial recordings. *Nat Commun* 8(1):1199.
5. Lafon B*, et al.* (2018) Author Correction: Low frequency transcranial electrical stimulation does not entrain sleep rhythms measured by human intracranial recordings. *Nat Commun* 9(1):949.
6. Opitz A*, et al.* (2016) Spatiotemporal structure of intracranial electric fields induced by transcranial electric stimulation in humans and nonhuman primates. *Sci Rep* 6:31236.
7. Voroslakos M*, et al.* (2018) Direct effects of transcranial electric stimulation on brain circuits in rats and humans. *Nat Commun* 9(1):483.
8. Wach C*, et al.* (2013) Effects of 10 Hz and 20 Hz transcranial alternating current stimulation (tACS) on motor functions and motor cortical excitability. *Behav Brain Res* 241:1-6.
9. Jausovec N, Jausovec K, & Pahor A (2014) The influence of theta transcranial alternating current stimulation (tACS) on working memory storage and processing functions. *Acta Psychol (Amst)* 146:1-6.
10. Hoy KE*, et al.* (2015) The effect of gamma-tACS on working memory performance in healthy controls. *Brain Cogn* 101:51-56.
11. Helfrich RF*, et al.* (2014) Entrainment of brain oscillations by transcranial alternating current stimulation. *Curr Biol* 24(3):333-339.
12. Noury N, Hipp JF, & Siegel M (2016) Physiological processes non-linearly affect electrophysiological recordings during transcranial electric stimulation. *Neuroimage* 140:99-109.
13. Hill DN, Mehta SB, & Kleinfeld D (2011) Quality metrics to accompany spike sorting of extracellular signals. *J Neurosci* 31(24):8699-8705.
14. Vinck M, van Wingerden M, Womelsdorf T, Fries P, & Pennartz CM (2010) The pairwise phase consistency: a bias-free measure of rhythmic neuronal synchronization. *Neuroimage* 51(1):112-122.
15. Zanos TP, Mineault PJ, & Pack CC (2011) Removal of spurious correlations between spikes and local field potentials. *Journal of neurophysiology* 105(1):474-486.
16. Noury N & Siegel M (2017) Phase properties of transcranial electrical stimulation artifacts in electrophysiological recordings. *Neuroimage* 158:406-416.
17. Martin KA & Schroder S (2016) Phase Locking of Multiple Single Neurons to the Local Field Potential in Cat V1. *J Neurosci* 36(8):2494-2502.